Properties of one-dimensional quasilattices

Jian Ping Lu
Department of Physics, City College of the City University of New York, New York, New York 10031

Takashi Odagaki*
Department of Physics, Brandeis University, Waltham, Massachusetts 02254

Joseph L. Birman
Department of Physics, City College of the City University of New York, New York, New York 10031
(Received 7 August 1985)

We study the properties of one-dimensional quasilattices numerically and analytically. The geometrical properties of general one-dimensional quasilattices are discussed. The Ising model on these lattices is studied by a decimation transformation: The critical temperature and critical exponents do not differ from those for a regular periodic chain. The vibrational spectrum in the harmonic approximation is analyzed numerically. The system exhibits characteristics of both a regular periodic system and a disordered system. In the low-frequency region, the system behaves as a regular periodic system; wave functions appear extended. In the high-frequency region, the spectrum is self-similar and there is no unique behavior for the wave functions. The spectrum shows many gaps and Van Hove singularities. The gaps in the spectrum are also obtained analytically by examining the convergence of a continued-fraction expansion plus decimation transformation. The energy spectrum of a tight-binding electron Hamiltonian on the Fibonacci chain is also analyzed; it shows similar characteristics to those of the lattice vibration spectrum.

I. INTRODUCTION

The discovery of icosahedral symmetry in a binary alloy of Al and Mn by Shechtman, Blech, Gratias, and Cahn[1] has opened a new era in condensed matter physics. Immediately after the discovery, Levine and Steinhardt[2] proposed a model which explains how icosahedral symmetry can coexist with long-range order: a crystal-like structure which gives sharp x-ray diffraction peaks. Since then several workers gave arguments based on Landau phase transition theory which showed that an icosahedral symmetry structure could be favored over the bcc structure in the quenching process.[3,4] Also the elastic properties were discussed based on Landau theory.[5] However, at present no experiment strongly supports any particular model.

In their paper Levine and Steinhardt proposed a three-dimensional Penrose tiling[6,7] as the basic structure for the icosahedral crystal. There are two distinguishing features in their model: First, for any given finite length there are many local icosahedral symmetry centers with a range of symmetry larger then the given length; second, instead of a periodic order which cannot coexist with icosahedral symmetry, it is necessary for the new structure to have quasiperiodic order. In this paper we concentrate on this second feature and study the properties of general one-dimensional quasilattices.

II. GEOMETRY

A regular periodic one-dimensional lattice can be generated from one basic unit cell by translation (or induction). A general one-dimensional quasilattice can be generated from a finite set of basic cells by a generalized induction procedure as follows. Let $a_1, a_2, \ldots, a_g$ be g basic units. Define this original pattern as stage 0 of the sequence. Then stage $n+1$ of the sequence is obtained inductively from stage n by the following (concurrent) substitution rule:

$$\mathbf{a} \rightarrow M\mathbf{a} , \tag{1}$$

where $\mathbf{a}$ represents a column vector: $\mathbf{a}=(a_1,a_2,\ldots,a_g)^t$, where t is transpose; and $M=(m_{ij})$ is a $g\times g$ matrix with non-negative integer entries. The matrix M and its successive applications fully determine the sequence. In this paper our interpretation of the action of the (concurrent) substitution rule [Eq. (1)] is that at each stage a_j is replaced with $m_{j1}\ a_1$ followed by (or concatenated with) $m_{j2}\ a_2, \ldots,$ etc., for $j=1,2,\ldots,g$. Following are several examples:

$$M=\begin{bmatrix}1 & 1\\ 1 & 1\end{bmatrix} \Rightarrow AB \rightarrow ABAB \rightarrow ABABABAB \rightarrow ABABABABABABABA \rightarrow \cdots , \tag{2a}$$

$$M=\begin{bmatrix}1 & 1 & 1\\ 1 & 1 & 1\\ 1 & 1 & 1\end{bmatrix} \Rightarrow ABC \rightarrow ABCABCABC \rightarrow ABCABCABCABCABCABCABCABCABC \rightarrow \cdots , \tag{2b}$$

 ©1986 The American Physical Society

$$M=\begin{bmatrix}1 & 1\\ 1 & 0\end{bmatrix}\Rightarrow AB\rightarrow ABA\rightarrow ABAAB\rightarrow ABAABABA\rightarrow ABAABABAABAAB\rightarrow\cdots\ , \tag{2c}$$

$$M=\begin{bmatrix}1 & 2\\ 1 & 0\end{bmatrix}\Rightarrow AB\rightarrow ABBA\rightarrow ABBAAABB\rightarrow ABBAAABBABBABBAA\rightarrow\cdots\ , \tag{2d}$$

$$M=\begin{bmatrix}1 & 1\\ 2 & 0\end{bmatrix}\Rightarrow AB\rightarrow ABAA\rightarrow ABAAABAB\rightarrow ABAAABABABAAABAA\rightarrow\cdots\ , \tag{2e}$$

$$M=\begin{bmatrix}1 & 2\\ 1 & 1\end{bmatrix}\Rightarrow AB\rightarrow ABBAB\rightarrow ABBABABABBAB\rightarrow ABBABABABBABABBABABBABABABBAB\rightarrow\cdots\ . \tag{2f}$$

Notice that the first two cases of Eq. (2) are periodic structures: M has the property that all the elements in one column are the same. Hence, the determinant of M is zero: This is a sufficient condition for periodic structures. The other four cases are nonperiodic structures, but the structures generated are nonetheless fully deterministic and highly ordered. Furthermore, as the length of the pattern goes to infinity, the ratio between the total number of elements of different components approaches constant value.

Consider the simple case with two basic elements, A and B (i.e., $g=2$). Let $N_A^{(n)},N_B^{(n)}$ be the number of occurrences of elements A and B at stage n, respectively: They satisfy the following recursion relations:

$$\begin{aligned}N_A^{(n+1)}&=m_{11}N_A^{(n)}+m_{21}N_B^{(n)}\ ,\\ N_B^{(n+1)}&=m_{12}N_A^{(n)}+m_{22}N_B^{(n)}\ .\end{aligned} \tag{3}$$

As n tends to infinity, the limit $r=\lim_{n\rightarrow\infty}(N_A^{(n)}/N_B^n)$ exists and is given by

$$r=\frac{m_{11}-m_{22}+[(m_{22}-m_{11})^2+4m_{12}m_{21}]^{1/2}}{2m_{12}} \qquad (m_{12}\neq 0)\ . \tag{4}$$

For the examples given above, r has the following values with respect to Eq. (2a), Eq. (2c), Eq. (2d), Eq. (2e), and Eq. (2f), respectively:

$$r=1,\quad r=\frac{\sqrt{5}+1}{2},\quad r=1\ ,r=2\ ,r=\frac{\sqrt{2}}{2}\ . \tag{5}$$

We see that the number r need not be irrational for the generation of a quasiperiodic lattice.

The simplest example of a quasiperiodic lattice is the case of Eq. (2c), which is known as the Fibonacci sequence. The number $\tau=(\sqrt{5}+1)/2$ is the golden mean. If we implement A and B as two distances with respective lengths L and S such that $L/S=\tau$, the sequence can be obtained by a projection method from a two-dimensional square lattice.[8] However, not all quasilattices can be obtained by a projection method.

To distinguish the quasilattice from periodic lattices and random lattices we introduce the configuration number $C(n)$. It is defined as follows: Randomly pick a segment of length n cells, then the total number of possible configurations is $C(n)$. As is well known $C(n)$ is constant for a periodic lattice, and exponentially dependent on n for a random lattice. For the quasiperiodic lattice the upper bound for $C(n)$ we found is linear in n. Take the Fibonacci lattice as example. The argument is the following: For any n one can find m such that $F_{m-1}<n\leq F_m$, where F_m are the Fibonacci numbers ($F_0=1$, $F_1=1$, and $F_{m+1}=F_m+F_{m-1}$, for $m\geq 1$). By the deflation procedure the whole lattice can be regarded as consisting of S' and L' only. These have F_{m-1} and F_m cells, respectively. Since the first F_{m-1} cells in L' are in the same order as S', for any segment of length F_m the number of possible configurations is less than F_{m+1} which is certainly also an upper bound for $C(n)$. By the way m was chosen one knows that F_{m+1} is proportional to n, hence, the upper bound of $C(n)$ cannot excede linearity in n. Whether there is a better estimation than linear is not clear to us, and remains an open question. We expect similar results will hold for higher-dimensional quasilattices.

III. ISING MODEL

Consider a one-dimensional Ising chain with separation d_{ij} of successive spins, given by either L or S which is determined by Eq. (2c) with nearest-neighbor coupling either $-J_L$ or $-J_S$ [Fig. 1(a)]. The Hamiltonian and partition function are

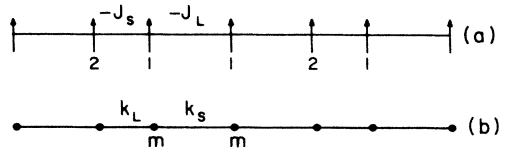

FIG. 1. (a) Quasiperiodic Ising chain with two different interaction constants $-J_L$ and $-J_S$. (b) Quasiperiodic harmonic chain. All atoms have the same mass and are connected by two different spring constants k_L and k_S.

$$H=-\sum_{ij=\mathrm{NN}} J_{ij}\sigma_i\sigma_j,\quad J_{ij}=\begin{cases}J_L & \text{if } d_{ij}=L\\ J_S & \text{if } d_{ij}=S\end{cases}\quad(\mathrm{NN}=\text{nearest neighbor}),\tag{6}$$

$$Z=\sum_{\{\sigma_i=\pm1\}}\exp[-\beta H(\{\sigma_i\})]=\sum_{\{\sigma_i,\sigma_j=\pm1\}}\exp\left[+\sum_{ij=\mathrm{NN}}K_{ij}\sigma_i\sigma_j\right],\quad K_{ij}=\beta J_{ij}=\frac{J_{ij}}{kT}.\tag{7}$$

We divide all spin variables into two sets, $\{\sigma_i^1\}$ and $\{\sigma_i^2\}$ [indicated by 1 and 2 in Fig. 1(a)]. Summing over all possible configurations of set 2, the partition function can be expressed in terms of new coupling constants K'_{ij} and spin variables of set 1. Apart from a constant factor, the new partition function has the same form as the original one. The renormalization transformation can be easily worked out

$$L'=L+S,\quad S'=L\,.\tag{8}$$

$$\tanh(K'_L)=\tanh(K_L)\tanh(K_S),\quad K'_S=K_L\,.\tag{9}$$

The renormalized system should have the same geometry as before; this requires $L'/S'=L/S$, or $L/S=\tau=(\sqrt{5}+1)/2$, which gives $L'=\tau L$; and $S'=\tau S$. The two fixed points are obvious. Denote $t=\tanh(K)$, then the fixed points are

$$t_L=t_S=t_c=0,\quad K_L=K_S=0,\quad T_c=\infty\,,\tag{10}$$

$$t_L=t_S=t_c=1,\quad K_L=K_S=\infty,\quad T_c=0\,.\tag{11}$$

Near the critical point $T_c=0$,

$$\begin{bmatrix}\Delta t'_L\\ \Delta t'_S\end{bmatrix}=\begin{bmatrix}1&1\\1&0\end{bmatrix}\begin{bmatrix}\Delta t_L\\ \Delta t_S\end{bmatrix}.\tag{12}$$

The two eigenvalues of the transformation matrix are $\lambda_{\max}=\tau$, $\lambda_2=-1/\tau$. The critical correlation length exponent ν is related to the largest eigenvalue

$$\nu=\frac{\ln\lambda_{\max}}{\ln b}=\frac{\ln\tau}{\ln\tau}=1\,,\tag{13}$$

where b is the geometrical scaling factor. We see that all these features are the same as in the case of the ordinary one-dimensional Ising lattice. The procedure carried out above does not depend on the particular lattice chosen. Rather it is the self-similarity property of quasiperiodic lattices that made it possible to carry out the renormalization transformation and that determines the form of recursion relations. Therefore, the result ($T_c=0$, $\nu=1$) should be valid for all one-dimensional quasiperiodic lattices. We have carried out the calculation for the general $g=2$ case, and the same results follow.

IV. VIBRATIONAL SPECTRUM

Consider a one-dimensional chain of atoms connected by harmonic springs. If the system is periodic, Bloch's theorem may be applied and, therefore, the solution of the equation of motion is wavelike, the phonon spectrum forms one or more bands, and the density of states is singular near the band edges. On the other hand, if the lattice is totally disordered, the wave function exhibits localization behavior, and the spectrum is a discrete set. However, as we pointed out in Sec. II the quasiperiodic lattice is intermediate between periodic and disordered, so it would not be surprising if it showed characteristics of both systems.

Let $u_n e^{-i\omega t}$ be the displacement of the nth atom from its equilibrium position and $k_{n,n+1}$ the spring constant connecting the nth to the $(n+1)$th atom and m_n the mass of the nth atom. The equation of motion is

$$-m_n\omega^2u_n=k_{n,n+1}(u_{n+1}-u_n)+k_{n-1,n}(u_{n-1}-u_n),\quad n=0,1,\ldots,N\,.\tag{14}$$

We are unable to solve a set of N of these equations analytically for quasiperiodic lattices. The difficulties come from the fact that the near-neighbor configurations of the nth atom cannot determine the near-neighbor configurations of the $(n+1)$st atom (but they are related) even though the number of types of near-neighbor configurations is a finite small set. However, by using the transfer matrix method[9] we have been able to obtain the spectrum numerically for N up to 8×10^3. Extensive calculations were carried out for the Fibonacci sequence and some calculations were also done for the other examples given in Sec. II.

Introducing a displacement vector (u_{n-1},u_n), one can write

$$\mathbf{u}_n=\begin{bmatrix}u_{n-1}\\ u_n\end{bmatrix}=\begin{bmatrix}a_n&b_n\\1&0\end{bmatrix}\begin{bmatrix}u_n\\ u_{n+1}\end{bmatrix}=\underline{T}_n\mathbf{u}_{n+1}\,,\tag{15}$$

where

$$a_n=1+\frac{k_{n,n+1}}{k_{n-1,n}}-m_n\frac{\omega^2}{k_{n-1,n}},\quad b_n=-\frac{k_{n,n+1}}{k_{n-1,n}}\,.$$

For a finite chain of $N+2$ sites

$$\mathbf{u}_1=\underline{T}_1\underline{T}_2\cdots\underline{T}_{N-1}\underline{T}_N\mathbf{u}_{N+1}=\underline{A}\,\mathbf{u}_{N+1}\,.\tag{16}$$

To obtain the eigenfrequency we must impose a boundary condition. We will use the fixed ends boundary condition $u_0=u_{N+1}=0$.[10] Thus,

$$\begin{bmatrix}0\\u_1\end{bmatrix}=\begin{bmatrix}a_{11}&a_{12}\\a_{21}&a_{22}\end{bmatrix}\begin{bmatrix}u_N\\0\end{bmatrix}.\tag{17}$$

To have a nontrivial solution for u_N, ω must satisfy the eigenvalue equation

$$a_{11}(\omega)=0\,.\tag{18}$$

From the eigenvalue equation the spectrum and density of states are obtained. For large N these spectra should approach the true spectra of the infinite system.

Consider the case that all atoms are identical, i.e.,

$m_n = m$ for all n and there are only two different spring constants k_L or k_S [Fig. 1(b)], depending on whether the distance between two atoms is long or short as per the Fibonacci sequence. There are only three possible types of nearest-neighbor configurations for the Fibonacci chain, namely LS, SL, and LL. The corresponding matrices $\underline{T}_j$ are

$$SL: \ \underline{T}' = \begin{bmatrix} 1+\frac{k_L}{k_S}\left[1-\frac{m\omega^2}{k_L}\right] & -\frac{k_L}{k_S} \\ 1 & 0 \end{bmatrix}, \tag{19a}$$

$$LS: \ \underline{T}'' = \begin{bmatrix} 1+\frac{k_S}{k_L}-\frac{m\omega^2}{k_L} & -\frac{k_S}{k_L} \\ 1 & 0 \end{bmatrix}, \tag{19b}$$

and

$$LL: \ \underline{T}''' = \begin{bmatrix} 2-\frac{m\omega^2}{k_L} & -1 \\ 1 & 0 \end{bmatrix}. \tag{19c}$$

The matrix $\underline{A}$ is the product of N of these matrices with the particular order determined by the sequence. Numerical calculations were carried out for several different N ($100 \le N \le 8000$) with different values of $\lambda = k_L/k_S$.

The following conclusions are suggested from the results of numerical simulations:

(1) In the low-frequency region [$x \equiv m(\omega^2/k_S) \ll 0.1$], the spectrum and wave function behave almost identically as for the ordinary periodic lattice. The integrated density of states can be fitted by

$$D(\omega^2) \approx C(\omega^2)^{1/2}, \tag{20}$$

where C is a constant (Fig. 2). The wave function looks essentially like a single harmonic periodic wave [Fig. 4(b)], suggesting that a long-wavelength wave propagates along the system with sound velocity proportional to the constant C. A simple estimate for C is just given by taking the geometrical average of the parameters involved, namely the lattice spacing and spring constant, then treating the system as periodic with these averaged parameters. This gives $C = \tau/(2\pi\sqrt{1+\tau\lambda})$. The fit is shown in Fig. 2,

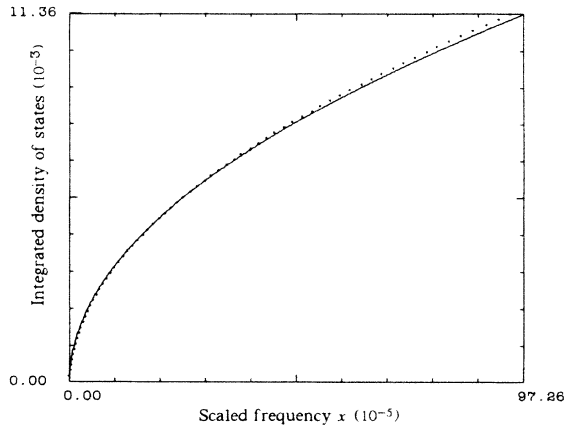

FIG. 2. Integrated density of states in the low-frequency region with $\lambda = (\sqrt{5}-1)/2 \approx 0.618$ (see also Fig. 3). The solid line is fitted by Eq. (20) with C given by the average estimation as in text. The system size is 4000 atoms. The horizontal axis is scaled frequency $x = m\omega^2/k_S$, and the integrated density of states is normalized to 1.

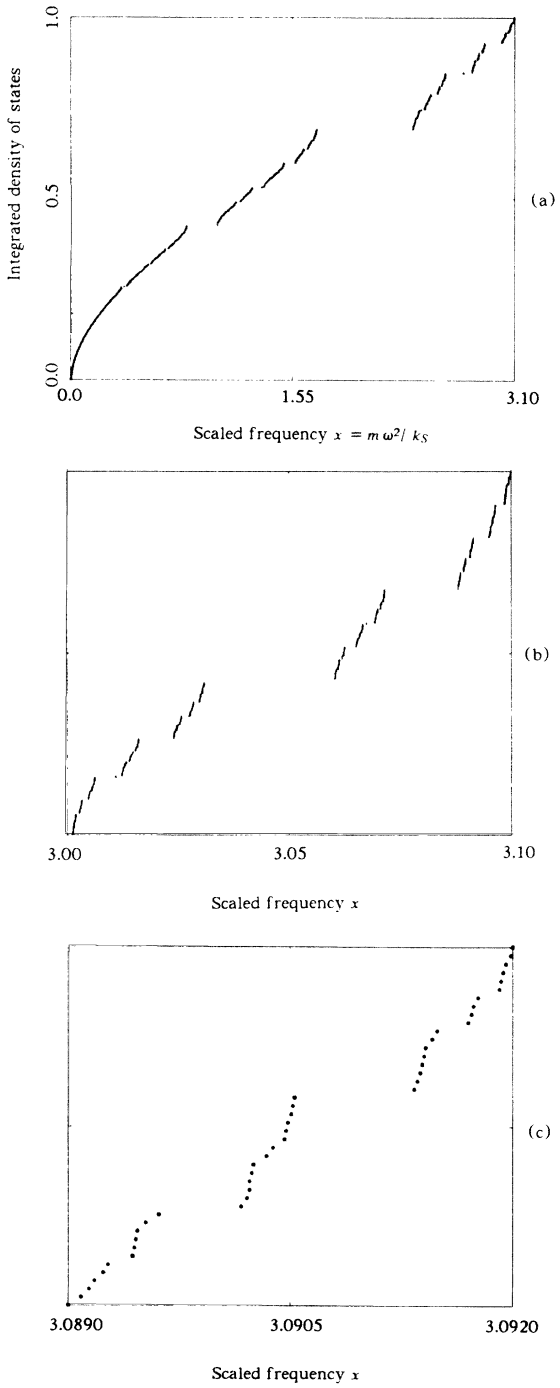

FIG. 3. (a) Integrated density of states for the Fibonacci chain of 2000 atoms with $\lambda = (\sqrt{5}-1)/2$. The coordinates are the same as in Fig. 2. (b) is the same as (a), enlarged around $x = 3.10$. (c) is the same as (b), further enlarged around $x = 3.0905$. Self-similarity is clear.

and the agreement is good.

(2) Careful examination of our results shows that the spectrum is self-similar. The self-similarity is more explicit in the high-frequency region (Fig. 3). From this we conjecture that the spectrum is "Cantor-like" for an infinite system. The spectra are bandlike if one neglects small gaps which may not be experimentally distinguishable. Near the edges of these "bands" the density of states exhibits Van Hove singularities.[11] The general structure of the spectrum will be discussed in the next section.

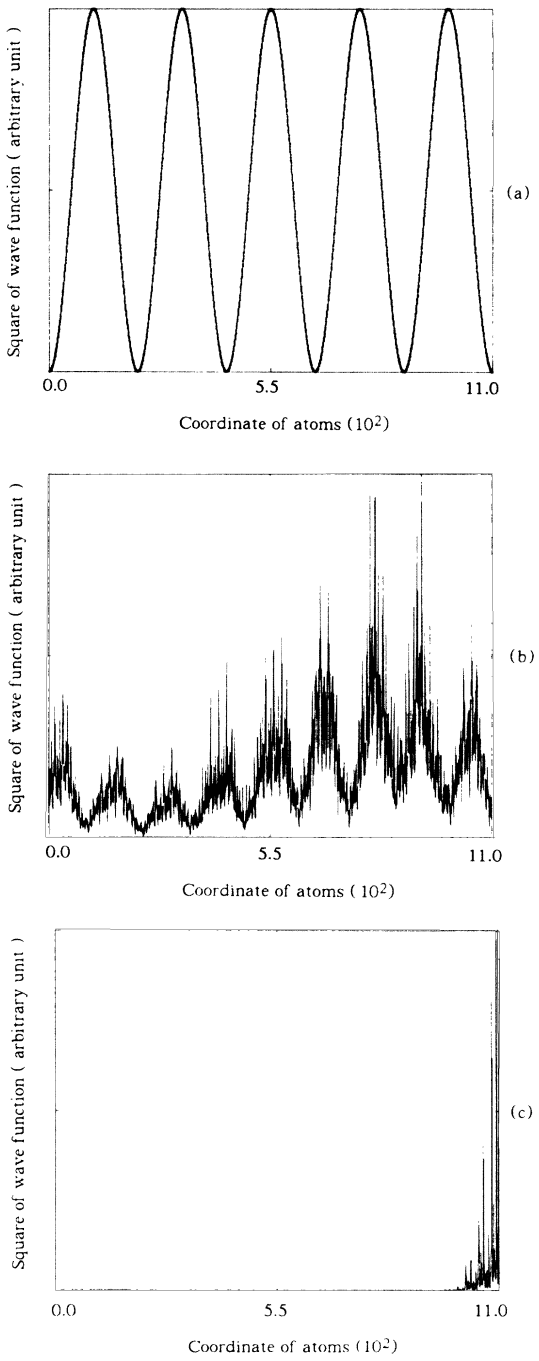

FIG. 4. Wave function for $\lambda=k_L/k_S=(\sqrt{5}-1)/2$ and 8000 atoms. The vertical axis is the square of the wave function (arbitrary unit), and the horizontal axis is the atomic coordinate [$L=1.0$, $S=1/\tau=(\sqrt{5}-1)/2$]. (a) $x=m\omega^2/k_S=0.279\times10^{-5}$. It is a wavelike extended state. (b) $x=0.627$. There is some indication of localization. (c) $x=3.04$, near the upper bound of spectrum. Obviously the state is localized at the right end.

(3) In general, the wave functions have three different types of behavior: (a) extended, (b) localized, (c) between types (a) and (b) (Fig. 4). Some workers[12] call type (c) critical. Generally speaking, the wave function is extended for very low frequencies and tends to be localized for high frequencies. However, we do not find any region in which all wave functions are localized. In fact, most wave functions are critical.

(4) For different quasilattices the qualitative features are the same, although the detailed distribution of gaps are different.

Similar spectra and wave functions have been observed in the one-dimensional incommensurate system. In the work of Kohmoto *et al.*[13] and Ostlund *et al.*[14] the tight-binding Hamiltonian obtained from a periodic potential was studied. By choosing a specific discontinuous periodic potential whose period is incommensurate with the lattice period, they have reduced the problem to a product of transfer matrices which follow the Fibonacci sequence. However, their transfer matrices are quasiperiodic only in the diagonal matrix element which originated from the potential in the Schrödinger equation. Another difference is that they used a periodic boundary condition which permitted reduction to one-dimensional mapping. Obviously that system is different from our system. Nonetheless the qualitative features of the spectra are the same. This may be due to universality.

V. STRUCTURE OF THE SPECTRUM

As we pointed out in the preceding section, in the limit $N\rightarrow\infty$ there are an infinite number of gaps in the spectrum, the integrated density of states is self-similar, and the spectrum is "Cantor-like." To further support this point, in this section we will develop a new technique which combines the continued-fraction expansion method and the decimation method, to examine the spectra.

Let us introduce dimensionless parameters $x\equiv m(\omega^2/k_s)$ and $\lambda\equiv k_L/k_S$. We first carry out numerical calculations of the spectrum for different λ ranging from 0 to 1.0 [Fig. 5(a)]. For $\lambda=0.0$, namely $k_L=0.0$, the chain breaks into isolated atoms and islands of two atoms connected by k_S, hence, the only possible eigenvalues are $x=0$ or 2. On the other hand, for $\lambda=1.0$ the chain becomes a monatomic chain connected by the same spring constant. In this case no gap should appear. Define z_i by

$$\frac{u_{i-1}}{u_i}=a_i+b_i\frac{u_{i+1}}{u_i}=a_i(1+z_i)\ , \tag{21}$$

where (a_i,b_i) are functions of x and λ. Then z_i can be written as

$$z_i=\frac{b_i a_i^{-1}a_{i+1}^{-1}}{1+z_{i+1}}=\frac{\rho_i}{1+z_{i+1}}\ , \tag{22}$$

where $\rho_j\equiv b_j a_j^{-1}a_{j+1}^{-1}$. One can then write

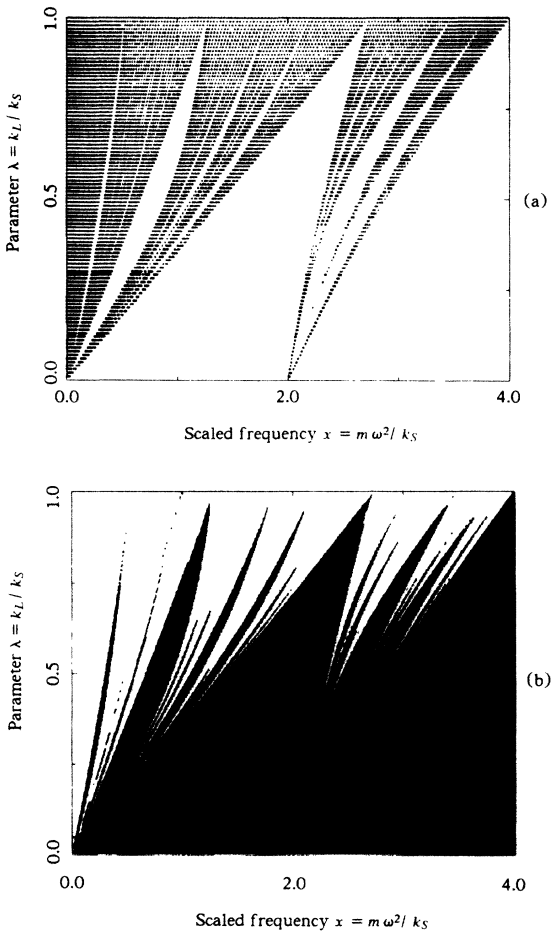

FIG. 5. Phase diagram of the vibrational spectrum for the Fibonacci chain. The horizontal axis is $x=m\omega^2/k_S$ and the vertical axis is the relative strength of the spring constant $\lambda=k_L/k_S$. (a) The numerical results. White areas belong to the gap. (b) Gap regions (black area) predicted by Worpitzky's theorem with tenfold decimation. One can see that this diagram is almost the exact complement of (a).

$$z_1=\cfrac{\rho_1}{1+\cfrac{\rho_2}{1+\cfrac{\rho_3}{1+\ddots\,1+\cfrac{\rho_n}{z_{n+1}}}}}\,. \tag{23}$$

The boundary condition $u_0=u_{N+1}=0$ corresponds to $z_{N+1}=\infty$ and $z_1=-1$.

On the other hand, Worpitzky's theorem[15,16] states that for ρ_j a function of any variable over a domain D, if

$$|\rho_j|\le\tfrac{1}{4}\ \text{for all } j\,, \tag{24}$$

then (a) the continued fraction z_1 [Eq. (23)] converges uniformly over the domain D,

$$\text{(b)}\quad |z_1|\le\tfrac{1}{2}\,, \tag{25}$$

(c) the constant $\frac{1}{4}$ is the best constant that can be used in Eq. (24) and the relation (b) is the best domain of values of z_1. Let us apply this theorem to our problem: $z_1(x,\lambda)$ will not satisfy boundary conditions if $|\rho_j|\le\frac{1}{4}$ for all j. So Eq. (24) is a sufficient condition for x not to be part of the allowed spectrum, i.e. x is in a gap.

As pointed out in the preceding section, we can have three different types of transfer matrix, hence, we have three different sets of (a_i,b_i). Because of the special geometrical properties of the sequence, they can only give four different ρ_j (Fig. 6):

$$\rho_1=\frac{b_3}{a_3a_2},\ \rho_2=\frac{b_2}{a_2a_1},\ \rho_3=\frac{b_1}{a_1a_3},\ \rho_4=\frac{b_1}{a_1a_2}\,. \tag{26}$$

If we consider the original sequence, then a and b take following values, depending on the sequence:

$$SL:\ a_1=1+\lambda-x,\ b_1=-\lambda\,, \tag{27a}$$

$$LS:\ a_2=1+\frac{1}{\lambda}-\frac{x}{\lambda},\ b_2=-\frac{1}{\lambda}\,, \tag{27b}$$

$$LL:\ a_3=2-\frac{x}{\lambda},\ b_3=-1\,. \tag{27c}$$

For a given λ and x, if all the ρ_j satisfy Eq. (24) then the point belongs to the gap region. Note the condition is sufficient but not necessary; therefore, even if Eq. (24) is not satisfied, the point may still belong to a gap. By this procedure we only found a small portion of the gap regions obtained in the numerical study, i.e., the triangle formed by three points: (0, 2.0), (0, 4.0), and (1.0, 4.0) in Fig. 5.

As the sequence is self-similar, we have developed the

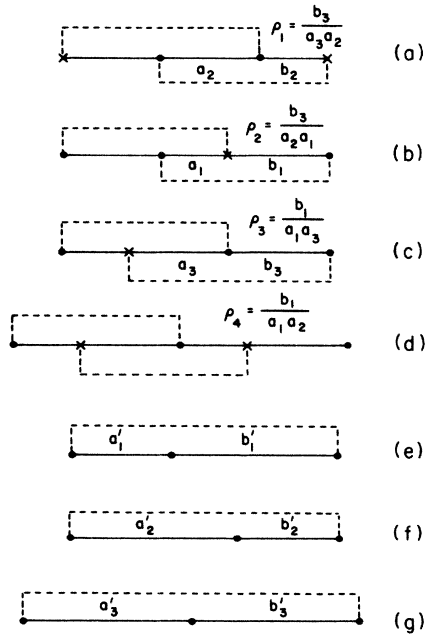

FIG. 6. Definition of (a,b) and the four possible combinations of ρ_j. (a) *LSS*, (b) *LSL*, (c) *SLL*, and (d) *SLSL*. Those sites labeled by a cross are to be decimated. After decimation the segments (b), (c), and (d) are shown in (e), (f), and (g), respectively, which define the new coefficients (a',b').

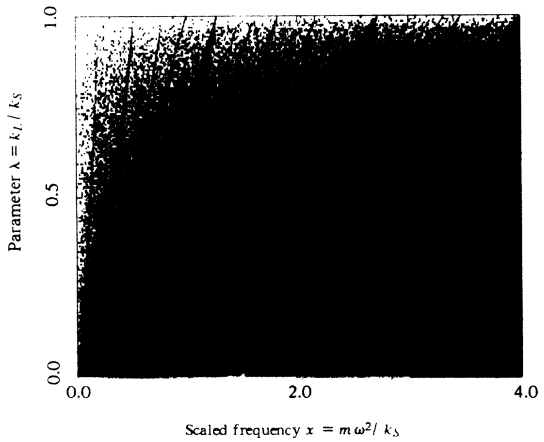

FIG. 7. Same as Fig. 5(b) but with 40-fold decimation: the gaps cover almost all the region of the diagram. This is a clear indication that the spectra are point sets. The triangular part formed by three points $A(3.0, 0.0)$, $B(4.0, 1.0)$ and $C(4.0, 1.0)$ is the gap region predicted by direct application of Worpitzky's theorem without a decimation transformation.

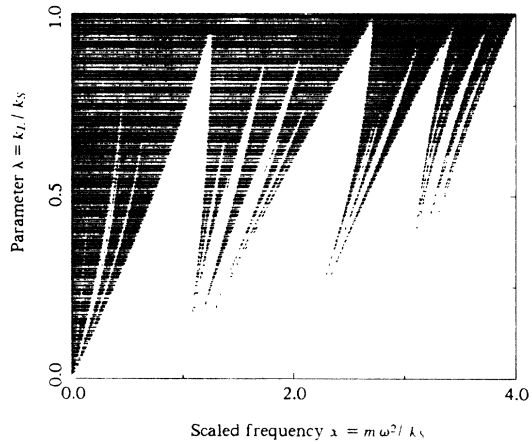

FIG. 8. Phase diagram of the vibrational spectrum for the Fibonacci lattice with the second type of implementation. The coordinates are the same as Fig. 5; the result is obtained by tenfold decimation.

decimation transformation similar to the procedures used in Sec. II. As an example, for the type of near neighbor shown in Fig. 6(b) one can write

$$u_{i-1}=a_2u_i+b_2u_{i+1},\quad u_i=a_1u_{i+1}+b_1u_{i+2}\ .$$

From these two equations one immediately obtains

$$u_{i-1}=\left[a_2+\frac{b_2}{a_1}\right]u_i+\left[-\frac{b_1b_2}{a_1}\right]u_{i+2}\ . \tag{28}$$

After decimation the sequence LSL becomes $S'L'$. Comparing Eq. (28) with Eq. (27) one gets new coefficients (a_1',b_1'). Similarly, the decimations change SLL and $SLSL$ to $L'S'$ and $L'L'$, respectively (Fig. 6). The recursion relations for (a,b) are the following:

$$\begin{aligned} &a_1'=a_2+\frac{b_2}{a_1},\quad b_1'=-\frac{b_1b_2}{a_1}\ ,\\ &a_2'=a_1a_3+b_1,\quad b_2'=a_1b_3\ ,\\ &a_3'=a_1a_2+b_1+b_2,\quad b_3'=-b_1b_2\ . \end{aligned} \tag{29}$$

The sequence after decimation has the same geometrical properties as the original sequence. Then (a_j',b_j') can form four different (ρ_j'). Hence, we can again apply Worpitzky's theorem to the new set of (ρ_j'). This procedure can be repeated. The result for decimations repeated ten times is shown in Fig. 5(b): The agreement with Fig. 5(a) is excellent. To confirm the conjecture we made before, namely that in the limit of an infinite system the spectrum is "Cantor-like", we show in Fig. 7 the result obtained by different numbers of decimations. One sees as n gets bigger the area of the gap region also gets bigger and eventually covers the whole plane. This is a clear indication the spectrum (unshaded area in Fig. 7) is a point spectrum.

The procedure just described is very efficient. For com-

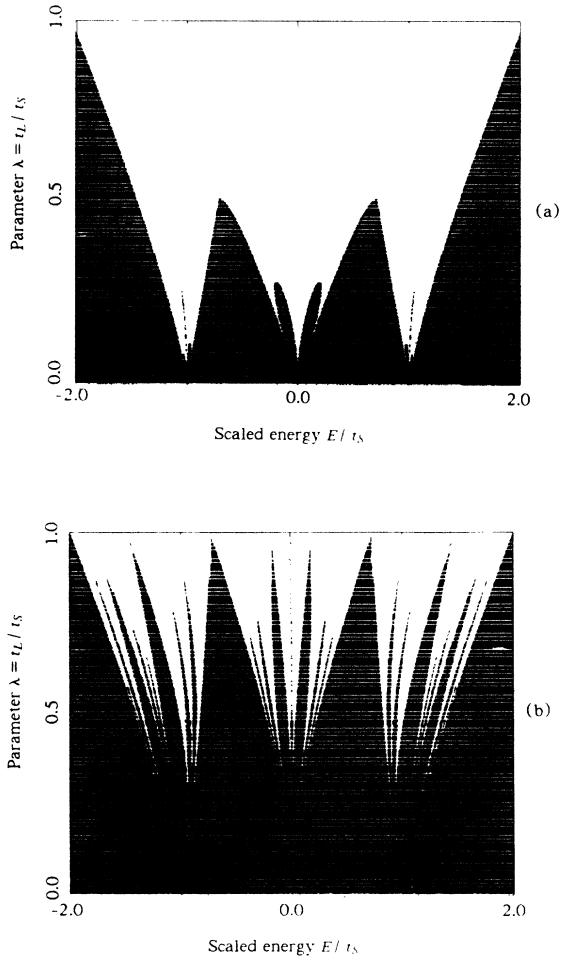

FIG. 9. Electronic spectrum. The shaded area is the gap predicted by continued fraction expansion and renormalization. The horizontal axis is $x=E/t_L$, and the vertical axis is $\lambda=t_L/t_S$. (a) Fourfold decimation. (b) Tenfold decimation.

parison, the CPU time needed to get Fig. 5(b) is 2 orders of magnitude less than that for Fig. 5(a), while the information is almost the same. The above result also favors the argument that the big gap region came from repeating a small unit cell. For example the segment AB appears an infinite number of times in the Fibonacci sequence; in fact, any segment of arbitrary length appears an infinite number of times in the infinite system. We have carried out successive approximations to the golden mean, that is the Fibonacci number. By treating the system as periodic with period F_n, one can see the splitting of the spectrum. Big gaps will be generated at the early stages of approximation and remain as gaps later on. The gap width changes but convergence is rapid. Similar calculations were done and the same results were observed before.[13]

In the above calculations the physical system implemented is that $A=L$, $B=S$, and we associated the two different spring constants k_L and k_S with these distances, respectively. This is not the only possible implementation: for example, one can take $A=S$, $B=L$ instead. The geometrical and the scaling properties of the sequence will not change, and the analyses carried out above are equally applicable. For example, in Fig. 8 we show a similar result, corresponding to Fig. 5. Note in this case there are combinations like SS but not LL in the sequence: hence, taking $\lambda=k_L/k_S=0$ breaks the sequence into segments of either two or three atoms connected by the same spring k_S. Therefore, the eigenvalues are $x=m\omega^2/k_S=0,1,2,3$. Mathematically this implementation is equivalent to the previous one if instead of λ changing from 0 to 1, λ changes from ∞ to 1. It is interesting to see how the spectra develop as λ changes. Starting with a two-point spectrum when $\lambda=0$, it develops into a continuous spectrum when λ reaches 1, and the spectrum becomes a four-point spectrum when $\lambda\rightarrow\infty$.

VI. ELECTRONIC SPECTRUM

Consider a tight-binding Hamiltonian

$$H=\sum_i |i-1\rangle t_{i-1,i}\langle i| + |i\rangle t_{i,i+1}\langle i+1| \ , \tag{30}$$

where $|i\rangle$ represents a Wannier state associated with site i, and t_{ij} is the nearest-neighbor hopping matrix. We can expand the electron wave function in terms of this orthogonal set

$$\Phi=\sum_i u_i |i\rangle \ . \tag{31}$$

Schrödinger's equation can be written as

$$Eu_i=t_{i-1,i}u_{i-1}+t_{i,i+1}u_{i+1}$$

or

$$u_i=\frac{E}{t_{i-1,i}}u_i-\frac{t_{i,i+1}}{t_{i-1,i}}u_{i+1}=a_iu_i+b_iu_{i+1} \ , \tag{32}$$

where E is the energy. Similarly to Eq. (27), one finds three different sets of (a,b)

$$a_1=x, \ \ b_1=-\lambda \ ,$$
$$a_2=\frac{x}{\lambda}, \ \ b_2=-\frac{1}{\lambda} \ , \tag{33}$$
$$a_3=\frac{x}{\lambda}, \ \ b_3=-1 \ ,$$

where $x=E/t_L$, $\lambda=t_L/t_S$; and t_L,t_S are similar to k_L,k_S in Sec. V. The analysis of the last section can be repeated but with the initial (a_i,b_i) of Eq. (33). The result is shown in Fig. 9. The characteristics of the spectrum are the same as the vibrational spectrum. This agrees with a computer simulation.[17] The conclusions drawn about the spectra and eigenfunctions in the last section are equally applicable.

VII. CONCLUSIONS

The analysis and calculations in the above sections can be carried over to general one-dimensional quasilattices in a straightforward way. The main conclusions should be the same. In summary, the quasiperiodic system reflects properties of both periodic and disordered systems. We have shown that quasiperiodicity is not necessarily related to irrationality of some physical parameter. The Ising model on a quasilattice belongs to the same universality class as the regular one-dimensional Ising model. The spectra (both phonon and electron) were shown to be "Cantor-like" by decimation calculations, and they possess characteristics of both periodic and disordered systems. On the one hand, it is a Cantor-like spectrum; on the other hand, it is bandlike and exhibits Van Hove singularities near the band edges if one neglects the small gaps. Similar spectral gaps and Van Hove singularities are also found in the Penrose tiling.[11,17] If the Penrose tiling model is a true basic structure for the new materials found, one needs a generalization of the present analysis to three dimensions in order to compare with experiments. However, we expect the qualitative features of the spectra will carry over to two-[16] and three-dimensional cases. Work on these problems is continuing for higher dimensions.

Note added. After this work was completed we received a copy of the work by Luck and Patribis,[18] which has some overlap with our work. Their results fully agree with ours. We thank T. C. Choy for calling our attention to this work.

ACKNOWLEDGMENTS

This work was supported in part by the National Science Foundation under Grant No. NSF-DMR-83-03981, and Professional Staff Congress—Board of Higher Education Grant No. PSC-FRAP-6-65280 at City College. The work at Brandeis University was supported in part by a grant from the Research Corporation (New York, NY). Discussions with Dr. Z. B. Su and Dr. Shirish M. Chitanvis were helpful.

*Also at GTE Laboratories, Waltham, MA 02254.

[1]D. Shechtman, I. Blech, D. Gratias, and J. W. Cahn, Phys. Rev. Lett. **53**, 1951 (1984).

[2]D. Levine and P. Steinhardt, Phys. Rev. Lett. **53**, 2477 (1984).

[3]Per Bak, Phys. Rev. Lett. **54**, 1517 (1985).

[4]N. D. Mermin and Sandra M. Troian, Phys. Rev. Lett. **54**, 1524 (1985); also M. V. Jarić, *ibid.* **55**, 607 (1985).

[5]D. Levine, T. C. Lubensky, S. Ostlund, S. Ramaswamy, P. Steinhardt, and J. Toner, Phys. Rev. Lett. **54**, 1520 (1985).

[6]R. Penrose, Bull. Inst. Math. Its Appl. **10**, 266 (1974).

[7]N. de Brujin, Ned. Akad. Weten. Proc. Ser. A **43**, 39 (1981); A. L. Mackay, Physica **144A**, 609 (1982); also see M. Gardner, Sci. Am. **236**, 110 (1977).

[8]P. Kramer and R. Neri, Acta Crystallogr., Sect. A **40**, 580 (1984).

[9]H. Matsuda, Prog. Theor. Phys., Suppl. **23**, 23 (1962).

[10]The other boundary condition one can use is the periodic boundary condition $\mathbf{u}_{N+1}=\mathbf{u}_1$. Then one gets the eigenvalue equation $\det[\underline{A}(\omega)-\underline{I}]=0$. The results are almost the same for both boundary conditions except for a small difference at very low frequency, and the difference vanishes as N gets larger. The physical reason behind this is clearly that for very low frequency the wavelength is long enough to be comparable with the length of the system we are numerical implementing. Hence, one expects the boundary condition to be important. Since we are interested in $N\rightarrow\infty$ limit, we will not further elaborate this point.

[11]T. C. Choy, Phys. Rev. Lett. **55**, 2915 (1985).

[12]S. Ostlund and R. Pandit, Phys. Rev. B **29**, 1394 (1984).

[13]M. Kohmoto, L. P. Kadanoff, and C. Tang, Phys. Rev. Lett. **50**, 1870 (1983).

[14]S. Ostlund, R. Pandit, D. Rand, H. J. Schellnhuber, and E. D. Siggia, Phys. Rev. Lett. **50**, 1879 (1983).

[15]H. Matsuda and K. Okada, Prog. Theor. Phys. **34**, 539 (1965).

[16]H. S. Wall, *Continued Fractions* (Van Nostrand, New York, 1948).

[17]T. Odagaki and Dan Nguyen, Phys. Rev. B **33**, 2184 (1986).

[18]J. M. Luck and D. Patribis (unpublished).

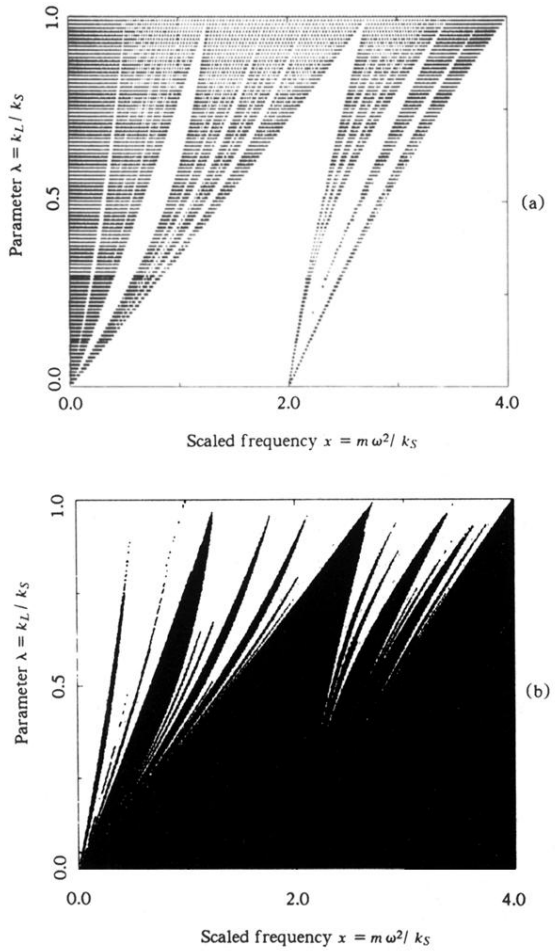

FIG. 5. Phase diagram of the vibrational spectrum for the Fibonacci chain. The horizontal axis is $x = m\omega^2/k_S$ and the vertical axis is the relative strength of the spring constant $\lambda = k_L/k_S$. (a) The numerical results. White areas belong to the gap. (b) Gap regions (black area) predicted by Worpitzky's theorem with tenfold decimation. One can see that this diagram is almost the exact complement of (a).

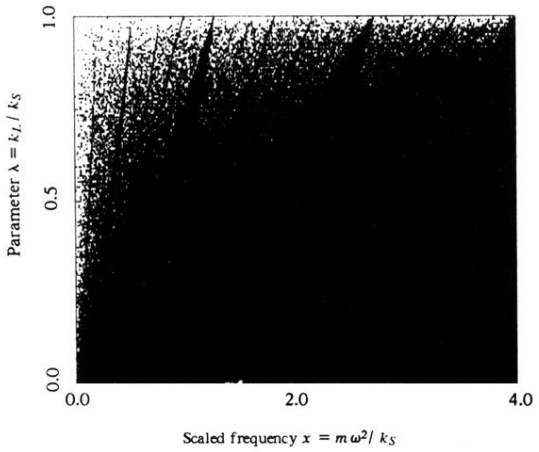

FIG. 7. Same as Fig. 5(b) but with 40-fold decimation: the gaps cover almost all the region of the diagram. This is a clear indication that the spectra are point sets. The triangular part formed by three points $A(3.0, 0.0)$, $B(4.0, 1.0)$ and $C(4.0, 1.0)$ is the gap region predicted by direct application of Worpitzky's theorem without a decimation transformation.

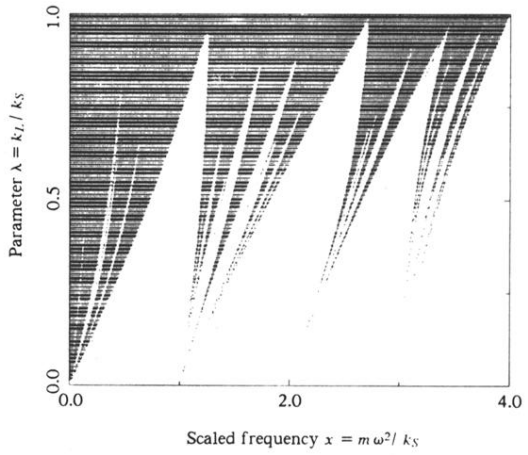

FIG. 8. Phase diagram of the vibrational spectrum for the Fibonacci lattice with the second type of implementation. The coordinates are the same as Fig. 5; the result is obtained by ten-fold decimation.

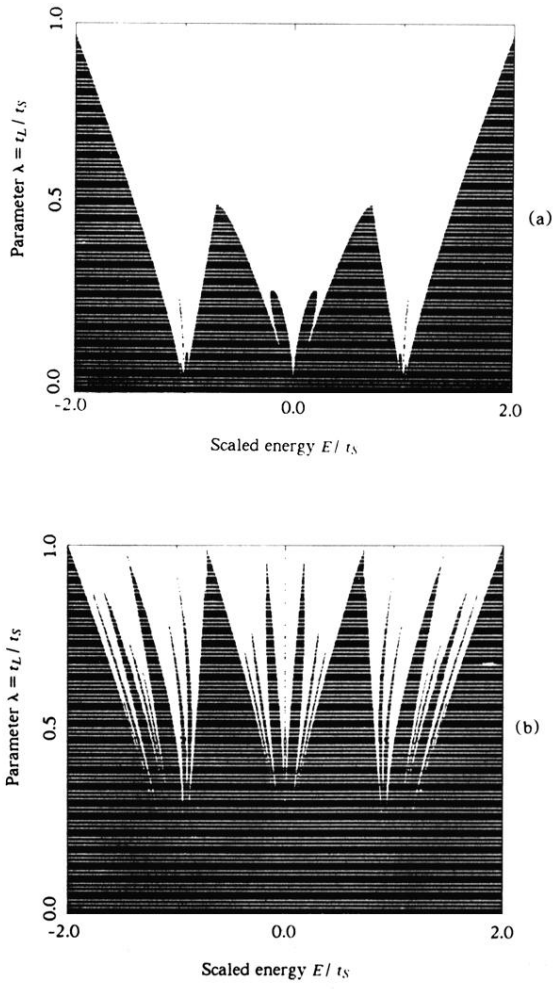

FIG. 9. Electronic spectrum. The shaded area is the gap predicted by continued fraction expansion and renormalization. The horizontal axis is $x = E/t_L$, and the vertical axis is $\lambda = t_L/t_S$. (a) Fourfold decimation. (b) Tenfold decimation.